

# Density Functional Theory Study of Solute Cluster Growth Process in Mg-Y-Zn LPSO Alloy

Mitsuhiro Itakura<sup>a</sup>, Masatake Yamaguchi<sup>b</sup>, Eiji Abe<sup>c</sup>, Daisuke Egusa<sup>c,d</sup>

<sup>a</sup> Center for Computational Science & e-Systems, Japan Atomic Energy Agency. 178-4-4 Wakashiba, Kashiwa, Chiba 277-0871, Japan

<sup>b</sup> Center for Computational Science & e-Systems, Japan Atomic Energy Agency. 2-4 Shirakata-Shirane, Tokai-mura, Naka-gun, Ibaraki 319-1195, Japan

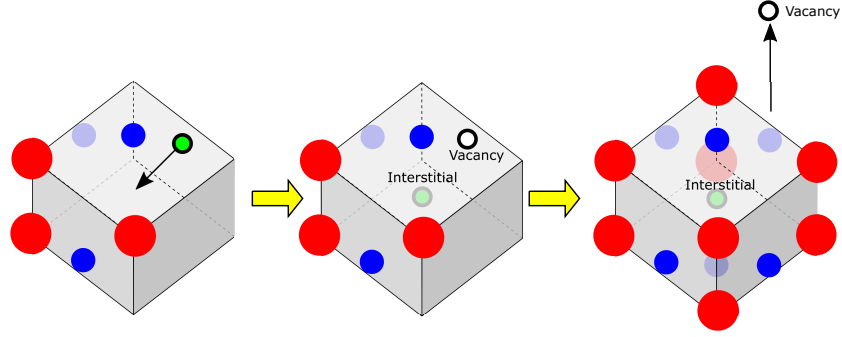
<sup>c</sup> Department of Materials Science and Engineering, University of Tokyo, Tokyo, Japan

<sup>d</sup> Research Center for Structural Materials, National Institute for Materials Science, Tsukuba, Japan

---

## Abstract

Solute cluster in LPSO alloys plays a key role in their idiosyncratic plastic behaviour such as kink formation and kink strengthening. Identifying the atomistic details of the cluster structure is a prerequisite for any atomistic modeling of LPSO alloys aiming for their improved strength and ductility, but there have been uncertainty about interstitial atom in the cluster. While density functional theory calculations have shown that inclusion of interstitial atom is energetically favorable, it has been unclear how the extra atom is provided, how much of the cluster have interstitial atoms, and what kind of element they are. In the present work we use density functional theory calculations to investigate the growth process of the solute cluster, specifically that of Mg-Y-Zn LPSO alloy, to determine the precise atomistic structure of solute cluster. We show that a pair of an interstitial atom and a vacancy is spontaneously created when a certain number of solute atoms are absorbed into the cluster, and all the full-grown cluster should include interstitial atom. We also show that interstitial atom is either Mg or Y atom, while Zn interstitial atom is extremely rare. These knowledge greatly simplifies atomistic modeling of solute clusters in Mg-Y-Zn alloy. Owing to the vacancies emitted from the cluster, vacancy density should be over-saturated in regions where solute clusters are growing, and the increased vacancy density accelerates cluster growth.



Graphical Abstract

## 1. Introduction

Solute cluster in Magnesium-based long period stacking order (LPSO) alloy [1, 2] plays a key role in their idiosyncratic plastic behaviour. Solute atoms form  $L1_2$ -type cluster [3] as shown in Fig. 1 and are strongly bound and displaced from original lattice positions, making it difficult for dislocations to cut through it and allowing only slips in the limited basal planes. While the lack of independent slip planes usually leads to poor ductility in most materials, LPSO alloys exhibit so-called "kink deformation" [4, 5, 6] which accomodates plastic deformation in various directions by structural organization of basal dislocations. It has been reported that these kink structures strengthen the material [7, 8, 9, 10, 11]. It is expected that there is much room for improvement of ductility and/or strength of LPSO alloys by optimizing their compositions and heat-treatment process. Atomistic modelling of the kink structure coupled with macroscopic model of plasticity should give guiding principles for the improvement, and various models have been proposed to account for the kink strengthening [12, 13, 14, 15].

Concerning atomistic modelling, there have been uncertainty of interstitial atom (IA) in the cluster. While density fucntional theory (DFT) calculations have shown that inclusion of interstitial atom is energetically favorable [16], it

has been unclear how the extra interstitial atom is provided, how much of the clusters have interstitial atoms, and what kind of element they are.

To answer these questions, we use DFT calculations to investigate the growth process of solute cluster, specifically that of Mg-Y-Zn LPSO alloy, to determine their precise atomistic structure. The elementary process of cluster growth is position exchange of solute atoms mediated by vacancy migration. We calculate energies of initial and final state of various elementary steps and estimate the rate of occurrence of each process from these energies. We will show that a pair of an interstitial atom and a vacancy is spontaneously created when a certain number of solute atoms are absorbed into the cluster, and all the full-grown cluster should include interstitial atom. We will also show that interstitial atom is either Mg or Y atom, while Zn interstitial atom is extremely rare.

The rest of this paper is organized as follows. In Sec.2, details of DFT calculations are described. In Sec.3, results of DFT calculations are presented. In Sec.4, consequences deduced from the obtained results are discussed. In Sec. 5, summary of the results and conclusions are shown.

## 2. Details of the calculations

### 2.1. Atomistic model

We investigate formation energies of single solute cluster embedded in a cell shown in Fig.2. Periodic boundary conditions are imposed in all directions, using a cell  $4\langle\bar{1}010\rangle \times 4\langle\bar{1}\bar{1}00\rangle \times 5\langle 0001\rangle$  which contains 10 basal layers and 480 atoms. For simplicity, we use atomistic configuration of almost isolated solute cluster, which corresponds to one fourth of the intra-plane cluster density of fully ordered LPSO structure, to avoid complexity of inter-cluster interactions.

In the present work, we focus on the formation process of solute cluster at stacking fault (SF) region. Each cluster is separated from its periodic image in  $\langle 0001\rangle$  direction by 6 basal Mg layers without solute atom, and we assume that the stacking order of these Mg layers does not affect cluster formation energy significantly. There are other choices for the cell such as 14H and 18R structures

[17, 18, 20, 19, 21, 22], but 10H structure is convenient to preserve hexagonal symmetry in calculations.

The cell size is determined by minimizing the total energy of 10H stacking structure without any solute atoms. The calculated cell size is characterized by lattice spacings  $a_0 = 3.19512$  and  $c_0 = 5.18991$ , which are slightly larger than that of hcp-Mg. Cell size is fixed to these values for all calculations and total energy is compared with each other. Each case exert different cell pressure, depending on the local expansion of the solute cluster configuration. The maximum cell pressure is about 40 MPa. We estimated the correction to the total energy coming from interaction between periodic images from cell pressure [23] and find that it is about 1 meV. We simply ignore this effect.

There are discussions on the relationship between SF formation and cluster growth, as each phenomena promotes the other and it is not clear which takes place first [24, 25]. In Mg-Y-Zn case, there is direct observation of solute segregation near dislocation cores of Shockley partials and subsequent growth of SF owing to Suzuki effect [26]. Therefore we assume that Y/Zn solute cluster grows on an existing SF and calculate cluster formation energy on SF of 10H structure.

## 2.2. DFT calculations

The electronic structure calculations and the structure relaxations by force minimizations in the DFT steps are performed using the Vienna Ab-initio Simulation Package (VASP) [27, 28] with the projector augmented wave method and ultrasoft pseudopotentials. The exchange correlation energy is calculated by the generalized gradient approximation (GGA) with the Perdew-Burke-Ernzerhof function [29]. The Methfessel-Paxton smearing method with 0.2-eV width is used. The cutoff energy for the plane-wave basis set is 360 eV, and the convergence of cluster binding energy with respect to the increasing cutoff is confirmed. Structural relaxation is terminated when the maximum force acting on the movable degrees of freedom becomes less than 10 meV/Å.

For the hexagonal supercell, k-points are placed on a Gamma-centered mesh

in the XY-plane to preserve the hexagonal symmetry and the Monkhorst-Pack k-point mesh is used in the Z direction. The number of k-points is  $2 \times 2 \times 2$  for all cases. We have confirmed that convergence of cluster formation energy with respect to the cut-off energy, k-point mesh size and system size is fast and errors are about 5 meV.

### 3. Results

Throughout the paper, we treat a vacancy as a type of solute element denoted by "V", and use expression such as "site A is occupied by V". A configuration of solute cluster is represented as  $\{Pi; Xi\}$ , where  $P_i$  denotes one of the sites shown in Fig.2 and  $X_i = Y, Zn, V$  denotes i-th solute atom which occupies the site. The binding energy of a cluster  $E_b(\{Pi; Xi\})$ , which is energy gain of cluster formation with respect to a configuration where each solute atom in the cluster is isolated, is calculated as follows:

$$E_b(\{Pi; Xi\}) = E_0(\{Pi; Xi\}) - E_0(0) - \sum_i E_1(Pi; Xi), \quad (1)$$

where  $E_0(\{Pi; Xi\})$  is the total energy of the cell of 10H structure containing the cluster,  $E_0(0)$  is total energy of 10H structure without any solute atoms, and  $E_1(Pi; Xi)$  is energy of single solute atom at site  $P_i$  calculated as follows:

$$E_1(Pi; Xi) = E_0(Pi; Xi) - E_0(0), \quad (2)$$

where  $E_0(Pi; Xi)$  is total energy of configuration in which single solute atom  $X_i$  substitutes position  $P_i$  in 10H structure.

When a cluster contains an IA, its formation process is pair creation of an IA and a vacancy, as we will show later. Therefore its reference state contains no IA and one less vacancies. Typically, if a cluster contains  $N_Y$  Y atoms,  $N_{Zn}$  Zn atoms and  $N_V$  vacancies and one IA in SF region, its reference energy is  $N_Y E_1(SF; Y) + N_{Zn} E_1(SF; Zn) + (N_V - 1) E_1(SF; V)$ . This equation holds regardless of the element species of IA, as well as when the cluster contains no vacancy.

Segregation energy of element X on SF, denoted by  $E_{SF}(X)$ , is calculated as  $E_{SF}(X) = E_1(P_{SF}; X) - E_1(P_{hcp}; X)$ , where position  $P_{SF}$  and  $P_{hcp}$  is located at SF and middle of three hcp layers. We find that  $E_{SF}(Y) = -0.10$  eV,  $E_{SF}(Zn) = -0.01$  eV, and  $E_{SF}(V) = 0.00$  eV.

Table 1 shows two-body solute-solute interaction energy  $E_b(P_1; X_1, P_2; X_2)$ . One can see that nearest neighbor Y-Zn interaction and next nearest neighbor Y-Y interaction is attractive, while all other interaction is very small. This result is consistent with the previous work calculated using either hcp or fcc lattice [30]. Table 2 shows binding energies of various clusters containing up to 6 solute atoms. It also shows measure of many-body interaction  $E_b - E_b^{(2)}$ , where  $E_b^{(2)}$  denotes cluster expansion energy calculated using only two-body interactions up to next nearest neighbors shown in Tab. 1. Table 2 also shows number of tetrahedral sub-clusters made of one Y atom and three Zn/V atoms. One can see that such tetrahedra exhibit significant many-body interaction and gain binding energy. Note that a fully formed  $Y_8Zn_6$  cluster has eight such tetrahedra and it is expected that cluster growth is promoted by formation of such tetrahedra.

Results shown in Tab. 2 indicate that vacancies are bound to the cluster as strongly as solute atoms, but relation between V absorption and solute absorption to the cluster needs careful consideration. Note that every migration of solute atoms is mediated by V diffusion. When a cluster absorbs a solute atom at a specific site, that site is first occupied by a vacancy, then that vacancy swaps its position with one of neighbor atoms. If that neighbor atom happened to be a solute atom, the solute atom is absorbed to the cluster.

The rate of V absorption to a specific site and V emission from that site, denoted by  $R(V^+)$  and  $R(V^-)$ , respectively, is given as follows:

$$R(V^+) = R_0 C_V, \quad (3)$$

$$R(V^-) = R_0 \exp(-|E_b^V|/kT), \quad (4)$$

where  $R_0$  is a V jump frequency in the bulk,  $C_V$  is an equilibrium V density in the bulk,  $E_b^V$  is a binding energy of V to the cluster (negative if attractive),

$k$  is Boltzmann's constant, and  $T$  is the temperature. In thermal equilibrium,  $C_V = \exp(-E_f^V/kT)$ , where  $E_b^V = 0.88$  eV is vacancy formation energy in the bulk evaluated by DFT calculation. If absolute value of V binding energy  $|E_b^V|$  is smaller than  $E_f^V$ , the site is occupied by V with probability  $R(V^+)/R(V^-) = \exp((|E_b^V| - E_f^V)/kT)$  in thermal equilibrium. In that case, the absorbed V quickly leaves the cluster and we can concentrate on the properties of clusters which only contain Y/Zn atoms when investigating the growth process of cluster.

We consider the rate of V emission followed by solute absorption, and that of inverse process, denoted by  $R(V^-S^+)$  and  $R(S^-V^+)$ , respectively. Their ratio is given as follows:

$$R(V^-S^+)/R(S^-V^+) = \frac{C_S \exp(|E_b^S|/kT)}{C_V \exp(|E_b^V|/kT)} \quad (5)$$

, where  $C_S$  denotes solute concentration in the bulk and  $E_b^S$  denotes solute binding energy (negative if attractive). Then the rate of solute absorption is given by  $R(S^+) = R(V^-S^+)R(V^+)/R(V^-)$ . Solute absorption is possible if  $R(S^+) > R(S^-V^+)$ , which gives

$$C_S \exp(|E_b^S|/kT) > 1. \quad (6)$$

For example,  $C_S = 0.01$ ,  $T = 500$  K and  $E_b^S < -0.2$  eV gives  $C_S \exp(|E_b^S|/kT) < 1$ .

When absolute value of V binding energy is greater than V formation energy, the site is occupied by V in most of the time. Assuming that solute binding energy is weaker than V binding energy, the rate of solute absorption and that of inverse process are given as follows:

$$R(V^-S^+) = R_0 C_S \exp((|E_b^S| - |E_b^V|)/kT), \quad (7)$$

$$R(S^-V^+) = R_0 C_V. \quad (8)$$

Solute absorption is possible if  $R(V^-S^+) > R(S^-V^+)$ , which gives

$$C_S \exp((|E_b^S| - |E_b^V| + E_f^V)/kT) > 1. \quad (9)$$

For typical case of  $C_S = 0.01$  and  $T = 500$  K, it gives  $|E_b^V| - |E_b^S| < 0.68$  eV. In that case, the site is first occupied by V and remain so in most of the time, until

solute atom comes at its neighbor site by diffusion and V swaps its position with solute atom.

As a cluster grows, Zn atoms at inner sites (a through f) tend to be displaced outwards, while Y atoms at outer sites (A through H) tend to be displaced inwards. The octahedral interstitial space at the center of the cluster becomes larger as the cluster grows, and after some threshold, it can accommodate interstitial atom. Figure 3 shows migration energy profiles of atoms moving from inner site to the interstitial site evaluated by nudged elastic band method [31] with 7 images. When three inner sites are occupied by Zn atoms, Mg atom at inner site can move to the interstitial site with energy barrier much lower than that of vacancy migration in the bulk, creating a pair of an IA and a vacancy with some energy gain. Zn atom at inner site can also move to the interstitial site, but with much larger energy barrier and less energy gain.

Table 3 shows binding energies of various cluster configurations and energy gain of IA-V pair creation. As the cluster grows, the energy barrier becomes lower and the energy gain becomes larger, and at some point, energy barrier banishes and configurations without IA become unstable. From these results, we conclude that every fully-grown cluster should contain IA. The IA atom is most likely to be Mg, and Zn interstitial is very unlikely because it has much higher energy barrier for its creation compared to Mg. While Mg and Zn atom have two stable positions at inner site and interstitial site, Y atom occupying inner site has only one stable position, and this stable position moves toward the interstitial site as other inner sites are occupied by Zn atoms, as shown in Fig. 4. Therefore it is possible that when one of the inner sites happened to be occupied by Y atom in the growth process, Y atom becomes an IA. Precise estimation of the ratio between Mg-IA and Y-IA requires detailed Monte Carlo simulations and it is out of scope of the present paper.

After the IA-V pair is created, V leaves the cluster if its binding energy is not comparable to the V formation energy  $E_f^V$ , as discussed before. If the binding energy of newly created V is comparable to  $E_f^V$ , it remains there until substituted by solute atom, provided that  $C_S \exp((|E_b^S| - |E_b^V| + E_f^V)/kT) > 1$ ,



as discussed before.

Figure 5 shows progression of cluster binding energy in the cluster growth process to the fully-formed cluster  $Y_8Zn_6$  plus IA. For a given configuration, energy gain of both Y and Zn absorption is investigated at sites where large energy gain is expected by forming new attractive pair of solute atoms and/or new solute tetrahedron composed of one Y and three Zn atoms. Then we choose a site and solute atom which has maximum absorption energy, include that atom to the cluster, and repeat the process. It is confirmed that all the absorption process satisfies the condition either  $|E_b^V| < E_f^V$  or  $C_S \exp((|E_b^S| - |E_b^V| + E_f^V)/kT) > 1$ .

Figure 6 shows absorption energy at various sites, including "wrong" absorptions such as Y absorption at inner sites and Zn absorption at sites other than inner or outer sites. Note that Zn absorption at outer sites does not create new Y-Zn neighbor pair and no energy gain is expected, so they are not included in the calculation. We only evaluate the case of Mg-IA. One can see that after IA is created, Y absorption at inner sites becomes highly unfavorable, promoting the proper absorption of Zn atoms at inner sites. After the IA is created, "right" absorptions tend to increase the number of  $Y_1Zn_3$  tetrahedra and are highly favorable.

#### 4. Discussion

We have shown that a pair of an interstitial atom and a vacancy is spontaneously created in the cluster growth process. It means that vacancy density becomes over-saturated in the region where solute cluster is growing. In such a situation, it is possible that vacancies accumulate at the solute cluster temporarily. Precise estimation of the effect of vacancy super-saturation on the cluster growth process requires mesoscopic scale simulation of vacancy density evolution, and it is out of scope of the present work.

More straightforward consequence is acceleration of cluster growth process, since the elementary process for the growth is vacancy diffusion and the growth rate is directly proportional to vacancy density. Normally, the growth rate of

the LPSO structure is expected to be proportional to  $\exp(-(E_f^V + E_m^V)/kT)$  where  $E_m^V$  is migration energy of vacancy. At the super-saturated region it can be accelerated to  $\exp(-E_m^V/kT)$ .

Another consequence of vacancy over-saturation is promotion of dislocation climb. When a Shockley partial dislocation absorb vacancies, it gradually moves in  $\langle c \rangle$  direction. Accelerated climb motion may help formation of periodic arrangement of SF.

In the growth process of LPSO structure, experimental observations indicate that the period of stacking order becomes shorter as LPSO structure is formed, and solute clusters follow the migration of stacking faults [17]. If cluster migration occurs by sequential migration of each solute atom, each migration removes a solute atom from the cluster and costs about 0.5eV, as shown in Fig. 6, indicating that such migration is quickly reverted. It is more plausible to assume that fully-grown cluster absorbs yet more solute atom to become a fused cluster [32], then a part of solute atom in the fused cluster leaves and becomes a  $L1_2$  cluster again, but at different position.

## 5. Conclusion

Using DFT calculations, we have investigated the mechanism of solute cluster growth in Mg-Y-Zn LPSO alloy, and found that a tetrahedral cluster made of one Y atom and three Zn atoms is highly stable. A fully-grown cluster contains eight such tetrahedra, and formation of such tetrahedra is a strong driving force for the cluster growth. Similar calculation of other combinations of rare-earth and transition metal elements will reveal the origin of different LPSO structures in various compositions. We also found that a pair of an interstitial atom and a vacancy is spontaneously created in the growth process, meaning that every fully-grown cluster contain interstitial atom. Interstitial atom is most likely Mg atom, and some portion can be Y atom, while interstitial Zn atom should be negligible. A vacancy created in the process is emitted from the cluster, and vacancy density should be over-saturated when the solute cluster is growing. This may promote dislocation climb and affect evolution of LPSO structure.

Mesososcopic modelling of cluster growth and vacancy emission, combined with modelling of dislocation glide/climb and stacking fault growth, is expected.

## 6. Acknowledgement

The authors are grateful to Hajime Kimizuka for his useful comments. This work was supported by JSPS KAKENHI for Scientific Research on Innovative Areas "Materials Science of a Mille-feuille Structure" (Grant Numbers 18H05480, 18H05479). Computations were performed on the ICEX at the Japan Atomic Energy Agency.

## References

- [1] Kawamura Y, Hayashi K, Inoue A, Masumoto T. Mater Trans 2001;42:1172-1176
- [2] Abe E, Kawamura Y, Hayashi K, Inoue A. Acta Mater 2002; 50:3845-3857
- [3] Egusa D, Abe E. Acta Mater 2012;60:166-178
- [4] Hagihara K, Yokotani N, Umakoshi Y. Intermetallics 2010;18:267-276
- [5] Yamasaki M, Hagihara K, Inoue SI, Hadorn JP, Kawamura Y. Acta Mater 2013; 61:2065-2076
- [6] Matsumoto T, Yamasaki M, Hagihara K, Kawamura Y. Acta Mater 2018;151:112-124
- [7] Hagihara K, Kinoshita A, Sugino Y, Yamasaki M, Kawamura Y, Yasuda HY, Umakoshi Y. Acta Mater 2010;58:6282-6293
- [8] Hagihara K, Kinoshita A, Fukusumi Y, Yamasaki M, Kawamura Y. Mater Sci Eng A 2013;560:71-79
- [9] Xu C, Nakata T, Qiao X, Zheng M, Wu K, Kamado S. Sci Rep 2017;7: 40846

- [10] Hagihara K, Li Z, Yamasaki M, Kawamura Y, Nakano T. *Acta Mater* 2019;163:226-239
- [11] Somekawa H, Ando D, Yamasaki M, Kawamura Y. *Materialia* 2020;:100786
- [12] Mayama T, Noda M, Chiba R, Kuroda M. *Int J Plasticity* 2011;27:1916-1935
- [13] Mayama T, Ohashi T, Tadano Y, Hagihara K. *Mater Trans* 2015;56: 963-972
- [14] Kobayashi S, Tarumi R. *Mater Trans* 2020; 61: 862-869
- [15] Inamura T. *Acta Mater* 2019; 173: 270-280
- [16] Saal JE, Wolverton C. *Acta Mater* 2014; 68: 325-338
- [17] Oñorbe E, Garcés G, Pérez P, Adeva P. *J Mater Sci* 2012; 47: 1085-1093
- [18] Kishida K, Yokobayashi H, Inui H, Yamasaki M, Kawamura Y. *Intermetallics* 2012;31:55-64
- [19] Hagihara K, Okamoto T, Izuno H, Yamasaki M, Matsushita M, Nakano T, Kawamura Y. *Acta Mater* 2016;109:90-102
- [20] Yamasaki M, Matsushita M, Hagihara K, Izuno H, Abe E, Kawamura Y. *Scr Mater* 2014; 78: 13-16
- [21] Kishida K, Nagai K, Matsumoto A, Yasuhara A, Inui H. *Acta Mater* 2015; 99:228-239
- [22] Tane M, Kimizuka H, Hagihara K, Suzuki S, Mayama T, Sekino T, Nagai Y. *Acta Mater* 2015;96:170-188
- [23] Varvenne C, Bruneval F, Marinica MC, Clouet E. *Phys Rev B* 2013;88:134102
- [24] Okuda H, Yamasaki M, Kawamura Y, Tabuchi M, Kimizuka H. *Sci Rep* 2015;5:14186

- [25] Mao P, Xin Y, Han K, Liu Z, Yang Z. Mater Sci Eng A 2020; 777: 139019
- [26] Hu WW, Yang ZQ, Ye HQ. Scr Mater 2016;117: 77-80
- [27] Kresse G, HafnerJ. Phys Rev B 1993;47:558
- [28] Kresse G, Furthmüller J. Phys Rev B 1996;54:11169
- [29] Perdew JP, Burke K, Ernzerhof M. Phys Rev Lett 1996; 77:3865-3868
- [30] Kimizuka H, Fronzi M, Ogata S. Scr Mater 2013; 69: 594-597
- [31] Mills G, Jonsson H. Phys Rev Lett 1994;72:1124
- [32] Kim JK, Ko WS, Sandl obes S, Heidelmann M, Grabowski B, Raabe D.  
Acta Mater 2016;112: 171-183

Table 1: Two-body binding energy between solute atoms for nearest neighbor and next nearest neighbor pairs in the stacking fault region. labels nn1, nn2, and nnn correspond to pairs shown in Fig.2. Energies are in unit of meV.

Solute pair	Y-Y	Zn-Zn	V-V	Y-Zn	Y-V	Zn-V
$E_b$ nn1	+94	+10	− <b>96</b>	− <b>52</b>	+68	− <b>35</b>
$E_b$ nn2	+151	+10	− <b>101</b>	− <b>77</b>	+35	− <b>38</b>
$E_b$ nnn	− <b>80</b>	−13	−6	−6	− <b>41</b>	+14

Table 2: Binding energy  $E_b$  for various clusters consisting of upto six solute atoms. Each cluster is labelled by the number of solute atoms (excluding vacancy) and index number. Letters A through H and a through f refer to positions shown in Fig. 1.  $E_b^{(2)}$  is binding energy estimated by cluster expansion using nearest neighbor pair energy and next-nearest Y-Y pair energy. All energies are in unit of meV.  $N_T$  denotes number of tetrahedra made of one Y and three Zn or V. Visualization of each configuration are available as supplementary materials.

Label	Y	Zn	V	$E_b$	$E_b - E_b^{(2)}$	$N_T$
C3-1	G	ac		-213	-56	
C3-2	b	ac		-202	-49	
C3-3	B	ab		-174	-45	
C3-4	B	ac		-132	-29	
C3-5	BC	b		-207	+1	
C3-6	BG	c		-234	-4	
C4-1	AB	ab		-377	-41	
C4-2	ACH	b		-351	+30	
C4-3	BG	ac		-406	-46	
C4-4	G	ace		-487	-250	1
C4-5	e	Edf		-445	-214	1
C4-6	B	abc		-367	-186	1
C3-7	B	ab	c	-480	-317	1
C5-1	ABe	ab		-372	+16	
C5-2	ABC	ab		-490	-22	
C5-3	AB	abc		-574	-185	1
C5-4	ACH	bd		-523	-11	
C5-5	BG	abc		-647	-210	1
C5-6	CH	bdf		-656	-216	1
C6-1	ABC	abc		-748	-152	1
C6-2	ABCH	ab		-723	+23	
C6-3	ABC	abe		-563	-95	
C5-7	ABC	ab	d	-569	-101	
C5-8	ABC	ab	c	-683	-216	1
C6-4	ABCe	ab		-446	+73	
C6-5	ABe	abc		-717	-145	1
C6-6	BGd	ace		-864	-171	1
C6-7	BGb	ace		-576	-35	1
C6-8	BCG	abc		-813	-167	1
C6-9	BG	abce		-939	-674	2

Table 3: Binding energy  $E_b$  for various clusters with and without IA. Each cluster is labelled by the number of solute atoms and index number. Letters A through H and a through f refer to positions shown in Fig. 1.  $\Delta E_{IA}$  is energy gain by the creation of IA-V pair. All energies are in unit of meV. Labels shown in the column of  $E_b$  means that the configuration is unstable and changes to the structure designated by the label. Visualization of each configuration are available as supplementary materials.

Label	IA	Y	Zn	V	$E_b$	$\Delta E_{IA}$
C4-1		AB	ab		-377	
C4-1i	Mg	AB	ab	d	C4-1	> 0
C5-3		AB	abc		-574	
C5-3i	Mg	AB	abc	e	-357	+217
C6-1		ABC	abc		-748	
C6-1i	Mg	ABC	abc	e	-808	-60
C6-9		BH	abce		-939	
C6-9i	Mg	BH	abce	d	C6-9	> 0
C6-10		AB	abcf		-812	
C6-10i	Mg	AB	abcf	e	-796	+16
C7-1		ABC	abcd		-997	
C7-1i	Mg	ABC	abcd	e	-1263	-266
C8-1		ABCD	abcd		C8-1i	
C8-1i	Mg	ABCD	abcd	e	-1647	< -300
C6-3		ABC	abe		-563	
C6-3i1	Zn	ABC	ab	e	-547	+16
C6-3i2	Mg	ABC	abe	f	C6-3	> 0
C6-3i3	Mg	ABC	abe	c	C6-3	> 0
C7-2		ABC	abce		-740	
C7-2i1	Zn	ABC	abc	e	-980	-240
C7-2i2	Mg	ABC	abce	d	-1053	-313
C6-4		ABCe	ab		-446	
C6-4i	Y	ABC	ab	e	C6-4	> 0
C6-5		ABe	abc		-717	
C6-5i	Y	AB	abc	e	C6-5	> 0
C7-3		ABCe	abc		-973	
C7-3i1	Y	ABC	abc	e	C7-3	> 0
C7-3i2	Mg	ABCe	abc	d	-419	+554
C8-2		ABCe	abcd		C8-2i	
C8-2i	Y	ABC	abcd	e	-1411	< 0
C9-1		ABCe	abcdf		C9-1i	
C9-1i	Y	ABC	abcdf	e	-2145	< 0



Table 4: Binding energy  $E_b$  for various clusters with IA. Each cluster is labelled by the number of solute atoms and index number. Letters A through H and a through f refer to positions shown in Fig. 1. All energies are in unit of meV. Visualization of each configuration are available as supplemental materials.

Label	IA	Y	Zn	V	$E_b$	$N_T$
C6-1i	Mg	ABC	abc	e	-808	1
C6-1i2	Mg	ABC	abc	d	-674	1
C6-1i3	Mg	ABC	abc		-363	1
C7-4i	Mg	ABC	abce		-630	1
C8-3i	Mg	ABCG	abce		-1240	2
C8-4i	Mg	ABC	abcde		-1026	1
C8-5i	Mg	ABCH	abce		-1057	1
C8-6i	Mg	ABCD	abce		-1048	1
C9-2i	Mg	ABCG	abcde		-1667	3
C9-3i	Mg	ABCGH	abce		-1703	2
C9-4i	Mg	ABCDG	abce		-1710	2
C10-1i	Mg	ABCGH	abcde		-2296	3
C10-2i	Mg	ABCDGH	abce		-2115	2
C11-1i	Mg	ABCGH	abcdef		-3071	5
C11-2i	Mg	ABCDGH	abcde		-2892	4
C12-1i	Mg	ABCDGH	abcdef		-3680	6
C13-1i	Mg	ABCDFGH	abcdef		-4257	7
C14-1i	Mg	ABCDEF GH	abcdef		-4662	8
C9-1i	Y	ABC	abcdf	e	-2145	3
C9-1i1	Y	ABC	abcdf		-835	3
C10-3i	Y	ABC	abcdef		-1602	3
C11-3i	Y	ABCD	abcdef		-2168	4
C11-4i	Y	ABCG	abcdef		-2203	4
C11-5i	Y	ABCH	abcdef		-2306	4
C12-2i	Y	ABCDH	abcdef		-2825	5
C12-3i	Y	ABCGH	abcdef		-2898	5
C13-2i	Y	ABCDGH	abcdef		-3477	6
C14-2i	Y	ABCDEGH	abcdef		-4029	7
C15-1i	Y	ABCDEF GH	abcdef		-4623	8

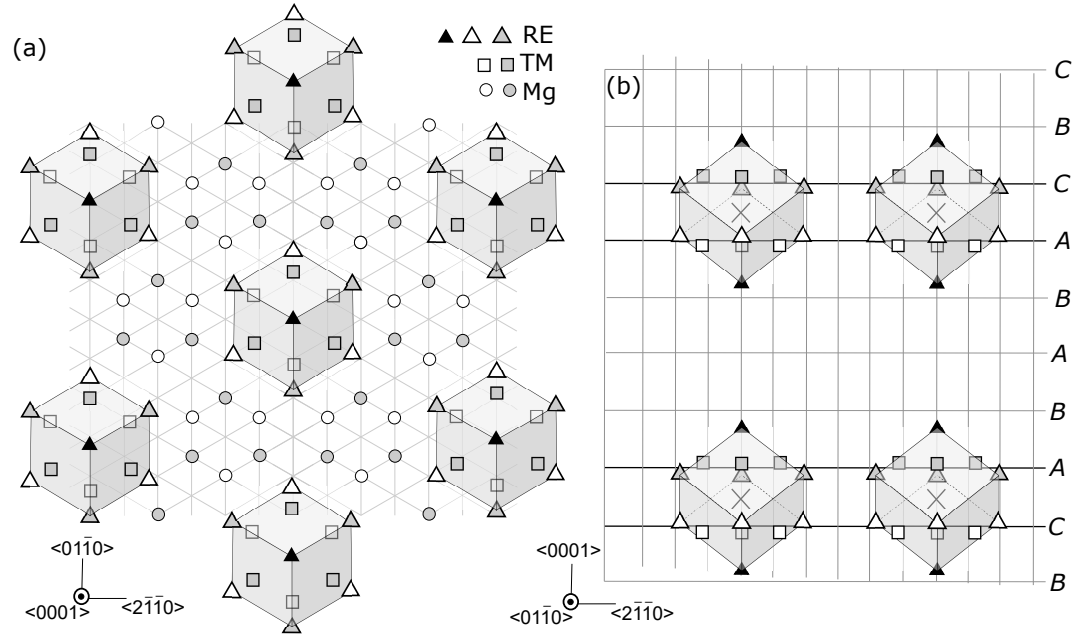
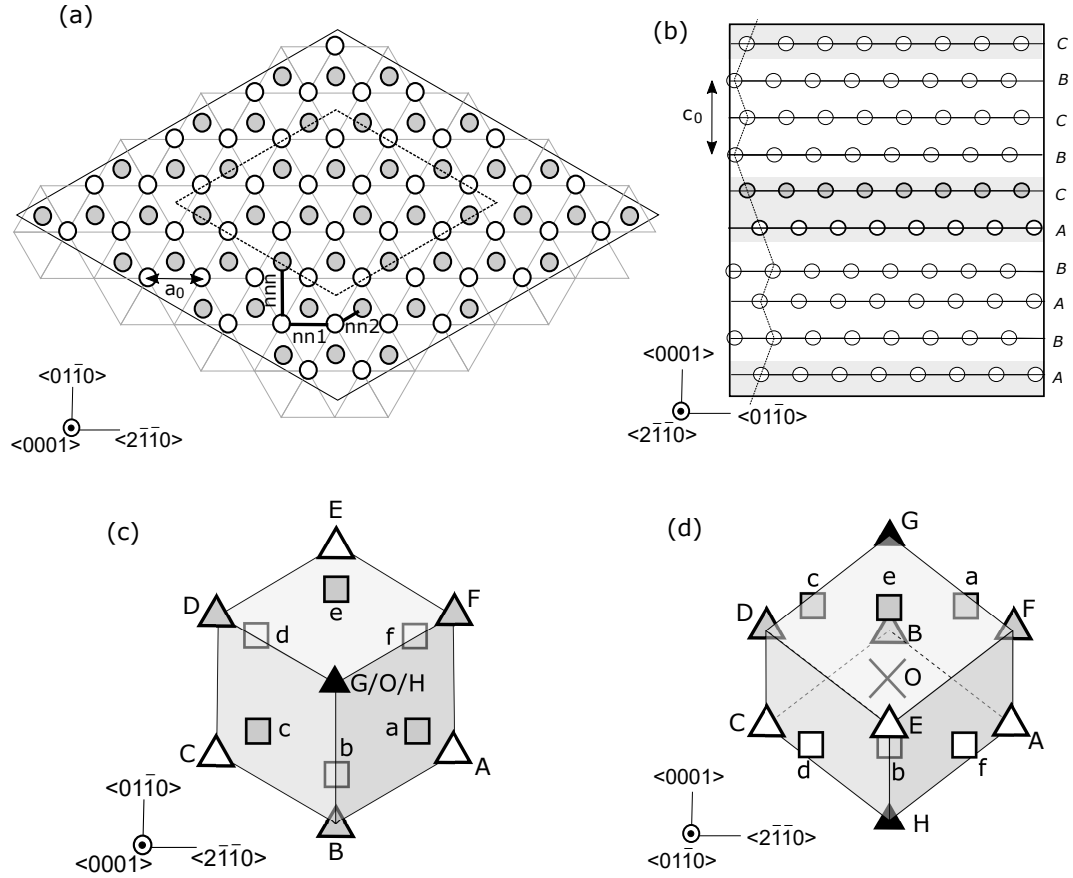


Figure 1: Typical atomistic structure of magnesium-based LPSO alloy, embedded in a 10H stacking structure, seen from (a)  $\langle 0001 \rangle$  and (b)  $\langle 01\bar{1}0 \rangle$ . Circle, triangle, and square symbols represent Mg, rare-earth and transition metal atoms, respectively. The color of symbols (white, gray, and black) indicate different basal layers. Each  $L_{12}$  cluster is embedded in a local fcc structure created by stacking faults shown by bold lines in (b). Letters A, B, and C in (b) indicate stacking order. Rare-earth atoms are located on the vertices of a cube and transition metal atoms are located on the center of faces of a cube. Rare-earth atoms are usually displaced toward the center of the cube from the original lattice positions, while transition metal atoms are displaced away from the center.



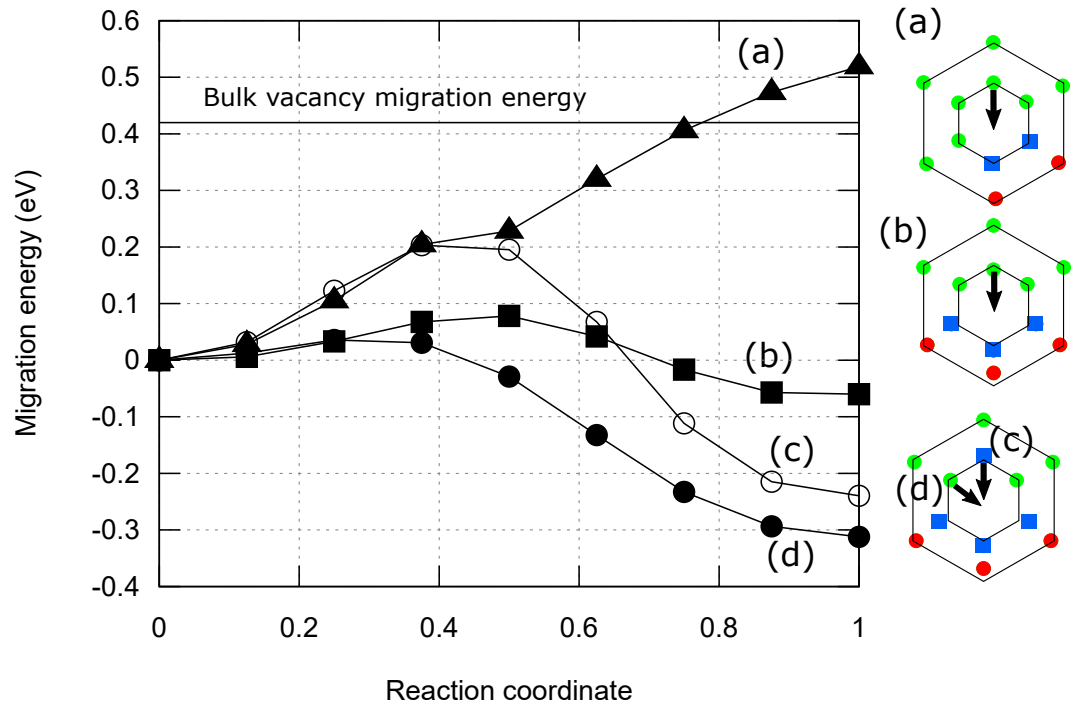


Figure 3: Energy profile of IA creation processes evaluated by nudged elastic band method. Migration energy of a vacancy in hcp Mg is also shown. Atomistic configuration for each plot (a) through (d) is shown on the right side. Green, red, and blue spheres correspond to Mg, Y, Zn atoms, respectively.

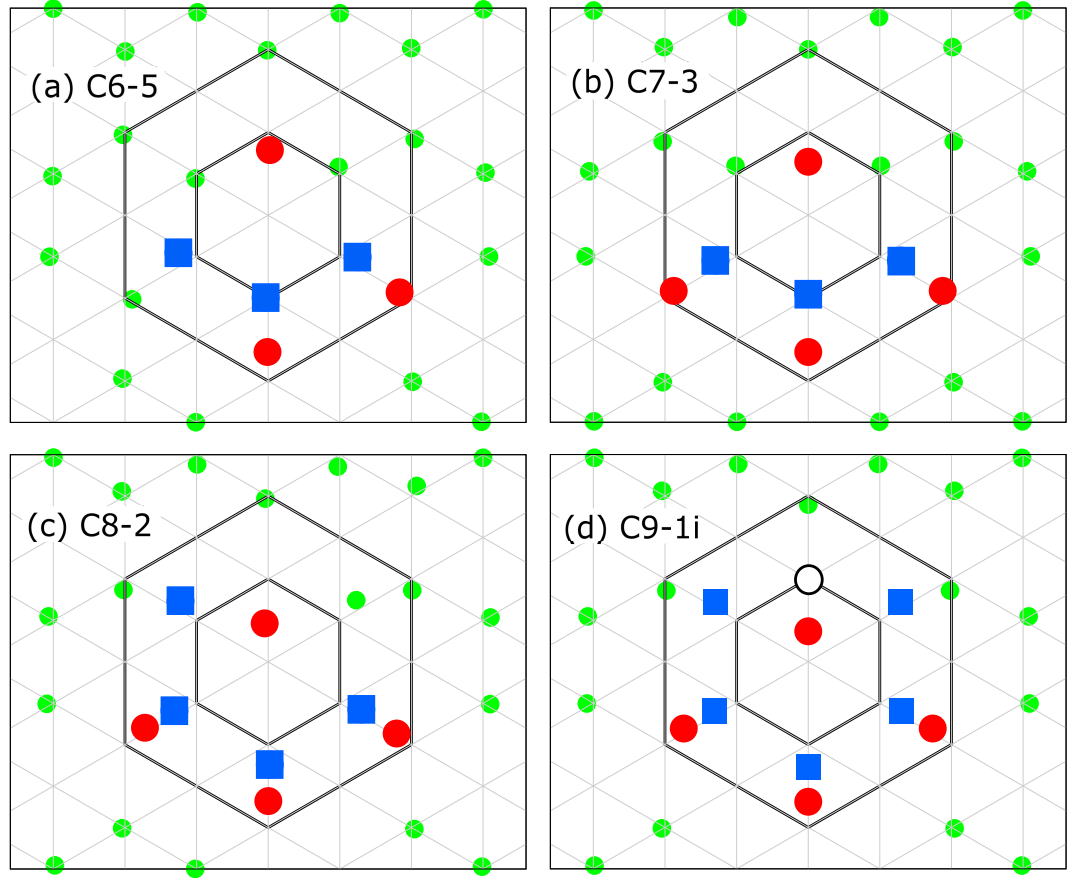


Figure 4: Atomistic configurations of several stages (a) through (d) of cluster growth process where Y atom gradually moves into the interstitial position. Green, red, blue, and white spheres correspond to Mg, Y, Zn, and vacancy, respectively.

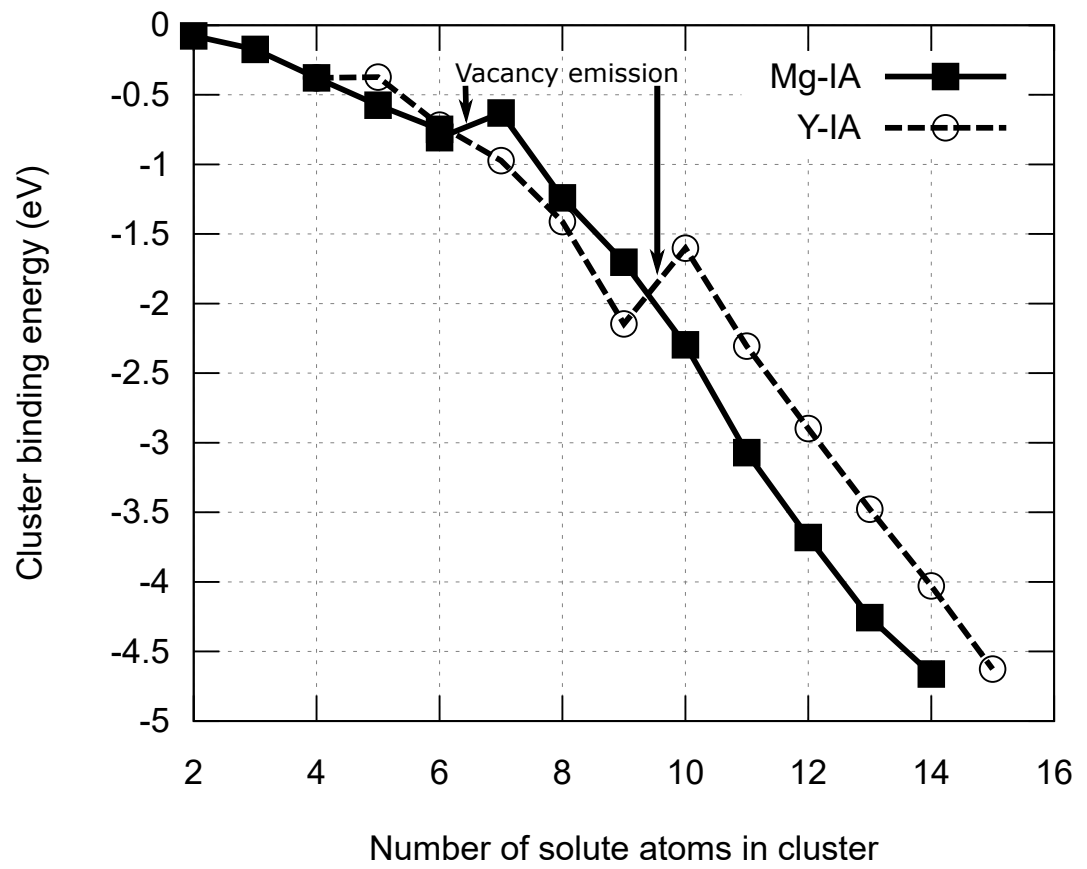


Figure 5: Progression of cluster binding energy during cluster growth process for two kinds of interstitial atom cases.

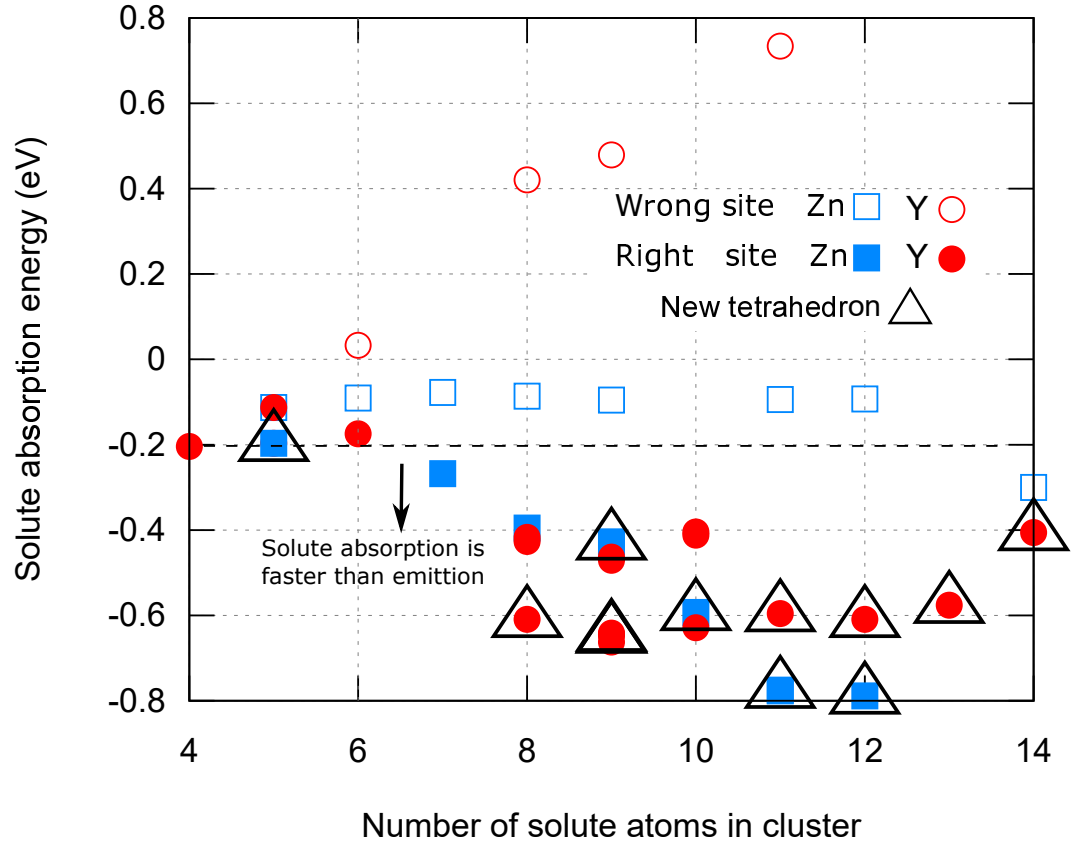


Figure 6: Solute absorption energy in the cluster growth process at various sites. "Right" site absorption means absorption of Zn atom at inner sites and Y atom at outer sites. "Wrong" site absorption means absorption of Y atom at inner sites and Zn atom at nearest neighbor sites of outer sites, excluding the inner sites. Absorption process which increases the number of  $\text{Y1Zn3}$  tetrahedra is marked with triangles.